JASMAC Conference of the Japan Society of Microgravity Application

OR3-2

炭素繊維強化プラスチックの対向流燃え拡がりにおける非燃焼部の熱的影響

Thermal Influences of Non-burned Zones on Opposed-flow Flame Spread over Carbon Fiber Reinforced Plastics

岡村康希 [1]，松川直生 [1]，松本圭佑 [1]，小林芳成 [2]，高橋周平 [2]
Koki OKAMURA[1], Naoki MATSUKAWA[1], Keisuke MATSUMOTO[1], Yoshinari KOBAYASHI[2], and Shuhei TAKAHASHI[2]
[1] 岐阜大学大学院自然科学技術研究科エネルギー工学専攻，Department of Energy Engineering, Graduate School of Natural Science and Technology, Gifu University
[2] 岐阜大学工学部機械工学科，Department of Mechanical Engineering, Faculty of Engineering, Gifu University

1. Introduction

Flame spread over solid materials has been extensively studied to investigate the effects of shape, thermophysical properties, and ambient atmospheres on the flame spread characteristics, such as flame spread rate, flammability limit, and so on. For example, Fernandez-Pello et al. investigated the effect of thickness of materials on flame spread rate[1]. Takahashi et al. examined the effect of ambient atmospheres and found that the flame spread rate reached the maximum under oxygen and argon mixtures[2]. These studies address polymers—e.g. polymethyl methacrylate (PMMA)—which are thermally isotropic mono-materials. Such materials have low thermal conductivity of less than 1 W/m/K, and therefore the solid-phase heat transfer is very small. However, there are some objects where the solid-phase heat transfer should be considered, for example, electrical wires consisting of polymer insulations and a metal core[3]. Flame spread over the electrical wires has been studied, while that over flat high-thermal-conductivity materials has not been well understood.

In recent years, carbon fibers (CFs) attract a lot of attention and are used extensively because they have superior properties, e.g., high strength, high electric conductivity, and low thermal expansion. Carbon fiber reinforced plastics (CFRPs) are an example of composite materials that consists of the CFs and applied to a variety of products. The CFs are found to have very high thermal conductivity, and therefore the CFRPs are also a high-thermal-conductivity material. However, the literature on flame spread over the CFRP is very limited, and therefore the flame spread behaviors are still not well understood.

In recent years, Kobayashi et al addressed the flame spread over thermally thin CFRP sheets and found that the preheat zone of CFRP is much larger than that of PMMA due to the high thermal conductivity of the CFs[4,5]. Matsukawa et al. investigated flame spread on CFRP sheets with different CF orientations, focusing on the effect of CF orientation on the flame spread characteristics[6]. However, these previous studies did not consider the effect of the left and right non-burned zone held by a sample holder. Probably, those zones would have a large influence on the flame spread characteristics because the solid-phase heat transfer sideways would vary

according to CF orientations. This work then studied the effects of non-burned zones on the flame spread over the CFRP sheets and modeled these effects to introduce to our developed CFRP flame spread model. Furthermore, the flame spread rates were computed and compared with the measured flame spread rates to validate the physical model of the non-burned zone.

2. Experiment

2.1. Carbon fiber reinforced plastic sheets with different carbon fiber orientations

The CFs are classified into two main types: polyacrylonitrile (PAN)-based CFs and petroleum pitch-based CFs. Their chemical structures are different, thereby resulting in different physicochemical properties. The pitch-based CFs have higher thermal conductivity than the PAN-based ones, and therefore the solid-phase heat transfer is greater in the flame spread over pitch-based CFRPs. This study then selected the pitch-based CFRPs as a test sample. A variety of differently oriented CFRP sheets, as illustrated in Fig. 2.1, were fabricated by laminating two unidirectional CF sheets impregnated with epoxy resins, i.e., prepregs (Nippon Graphite Fiber, NT91500-525S) in different direction and curing them in a high temperature furnace (Yamato Scientific, FO810) at 403 K (130 ℃) for 1h. CF orientations of those CFRP sheets are symmetric for longitudinal direction of CFRP sheets. Specifications of the used prepreg are listed in Table 2.1. The prepared CFRP sheets can be categorized as "thermally thin" because of the high thermal diffusivity of ~2.3 × 10^2 mm^2/s.

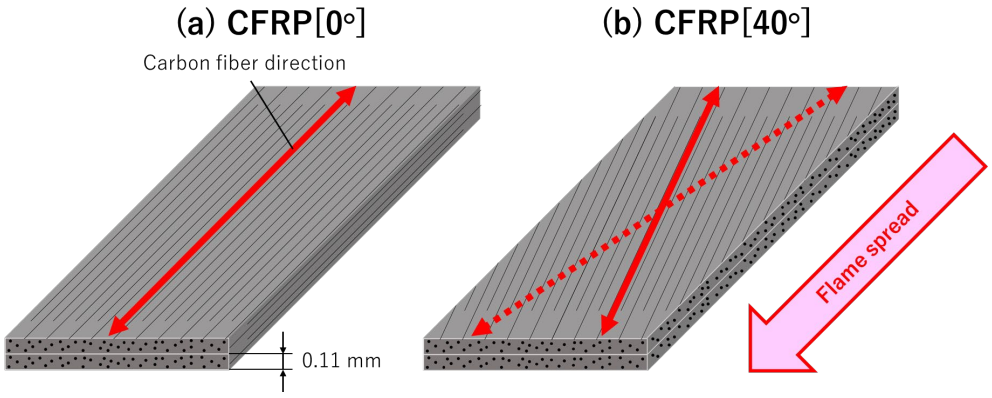

Fig. 2.1 Schematic of carbon fiber reinforced plastic (CFRP) sheets with different carbon fiber (CF) orientation: (a) CFRP [0°] and (b) [40°].

Table 2.1 Specifications of unidirectional CF sheets impregnated with epoxy resin.

Manufacturer / Model	Nippon Graphite Fiber / NT91500-525S
Type of carbon fibers	Mesophase pitch-based continuous carbon fibers
Type of thermosetting resins	Epoxy resins
Thickness	0.11 mm per sheet
Fiber areal weight	150 g/m^2
Resin content	25 wt.%
Thermal conductivity （CF）	500 W/m/K
Thermal conductivity （epoxy resin）	0.3 W/m/K

2.2. Apparatus for downward flame spread tests

The fabricated CFRP sheets were cut 12 cm long by 3 cm or 2 cm wide and inserted vertically into a stainless-steel sample holder (Fig. 2). Note that this work studied downward flame spread to facilitate an analysis as much as possible. The size of combustion part was 12 cm long by 2 cm wide. A 0.5-mm-thick nichrome wire was equipped with the sample holder to ignite the CFRP sheets. The nichrome wire was energized with 150 W (20 V × 7.5 A) and then turned off once a self-sustaining flame spread was recognized. Locating the sample holder with the CFRP sheets in the glovebox allowed oxygen concentration in the atmosphere to vary. The flame spread tests were conducted in variable oxygen concentrations at a total pressure of 0.1 MPa. Pressure and oxygen concentration were constantly monitored during the flame spread tests via a manometer (SIBATA, DM-1) and an oxygen meter (JIKCO, JKO-25LD3), respectively. Note that the glovebox was so large (1 × 1 × 1 m^3) that a decrease in oxygen concentration due to combustion was small enough to be negligible. This work defined "flame spread" if a flame could spread and reach the point which was 4 cm above from the bottom edge of the CFRP sheets and "no flame spread" if a flame was extinct before reaching the above point. Flame spread behaviors were recorded via a video camera (Sony, HDR-CX470), and the in-plane temperature distribution during flame spread was visualized via an infrared camera (Nippon Avionics, InfRec S25). The flame spread tests were repeated at least three times for each condition to quantitatively assess the experimental uncertainty.

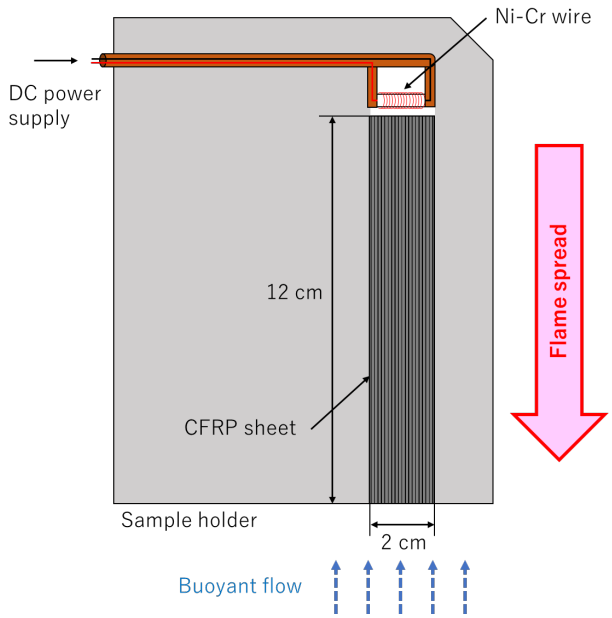

Fig. 2.2 Schematic of sample holder for buoyant flow downward flame spread tests.

3. Results

3.1. Flame spread behaviors

Fig. 3.1 shows that a large preheat zone was formed ahead of the flame and became more pronounced as the CF crossing angles was decreased. This indicates that the CFs act as a heat conductor to transfer the heats from the flame forward. The length of the preheat zone, i.e., the preheating length, for the CFRP sheets with a size of 3 × 12 cm was shorter

than that of those with a size of 2 × 12 cm. This is because the heats from the flame would leak sideways for the 3 × 12-cm CFRP sheets, and therefore smaller heats were transferred forward. For the 2 × 12-cm CFRP sheets, on the other hand, no heat leaks would make the preheating length longer. To better understand the flame spread behaviors of the CFRP sheets with an emphasis on the effects of non-burned zones, the direct and IR images were analyzed to produce the quantitative data. These data is further discussed in the following chapters.

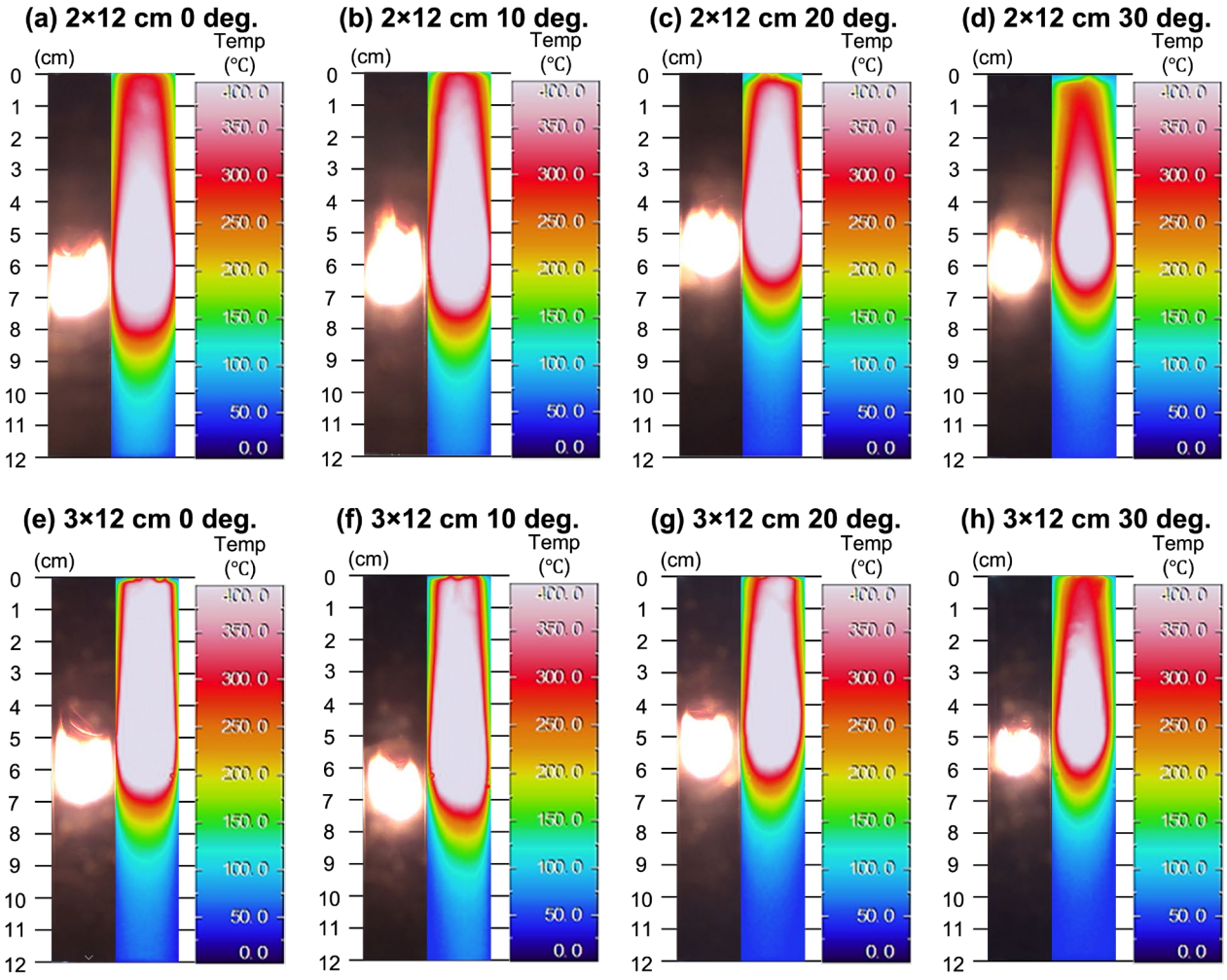

Fig. 3.1 Direct and IR images of downward flame spread behaviors of CFRP sheets with different CF orientations in an oxygen concentration of 60%: (a) – (d) CFRP [2 × 12 cm] and (e) - (h) CFRP [3 × 12 cm].

3.2. Flammability: Limiting oxygen concentration

The limiting oxygen concentrations (LOCs) of CFRP sheets are plotted as a function of CF orientation angle (i.e., the angle of prepreg relative to the other, θ) in Fig. 3.2. This work defined the LOC as the minimum oxygen concentration where flame spread was achieved. The LOC increased significantly with CF orientation angle, which agrees with the literature[6]. The sample holder holds 5 mm in both sides of CFRP [3×12cm], i.e., 1 cm in total, whereas CFRP [2×12cm] has such non-burned zones other than the combustion area. The CFRP [2×12cm] tends to require less heat to raise the temperature than the CFRP [3×12cm], resulting in smaller LOCs in tested CF orientation angles. This tendency becomes more remarkable as θ increases because more heats would be transferred sideways as heat loss.

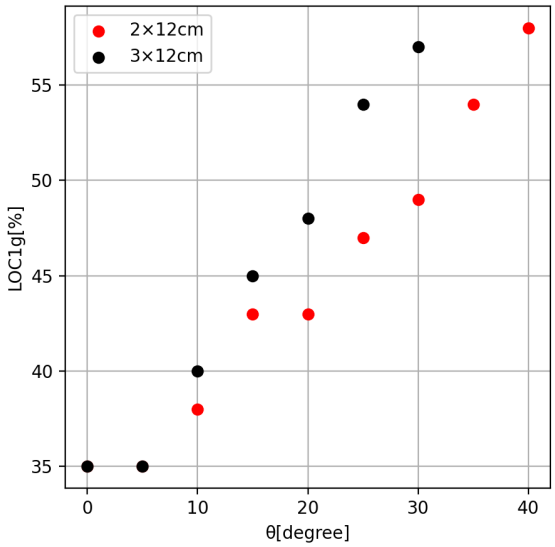

Fig. 3.2 Limiting oxygen concentration of CFRP sheets with different widths in buoyant flow as a function of CF orientation angle.

3.3. Solid-phase preheating length

To understand how the CFs work in the flame spread, the in-plane temperature distribution during flame spread was visualized via the IR camera. To quantify the solid-phase preheat zone, the length of the solid-phase preheat zone, i.e., the solid-phase preheating length (L_s), was measured by processing the IR images via an in-house Python image-processing code. Note that this work defined the distance from the flame's leading edge to the point where the non-dimensional temperature $\Theta = (T - T_\infty)/(T_v - T_\infty)$ reached a value of 0.3 as the representative L_s. If the pyrolysis and ambient temperatures (T_v and T_∞) are 670 K and 293 K, respectively, then L_s is the distance to the point at the temperature of 406 K. As shown in Fig. 3.3, L_s decreased with increasing $\theta$and oxygen concentration, which agrees with the past study[6]. At $\theta = 0$ deg., heats transfer rates in the direction of flame spread are high because no CF orientation angles do not allow heats to be transferred sideways. As θ is increased, however, heat transfer sideways become significant, resulting in lower heat transfer rates in the longitudinal direction. Consequently, L_s decreases with increasing θ. In addition, the effects of oxygen concentration can be understood by solving the one-dimensional unsteady heat conduction equation for a semi-infinite solid. The heat penetration distance in the solid phase, i.e., L_s in this work, is expressed as $L_s \propto \sqrt{\alpha_s t}$ where α_s and t are the thermal diffusivity and the characteristic time in the solid phase. Here, t is expressed as L_s/V_f, and therefore, L_s is rewritten as:

$$L_s \propto \frac{\alpha_s}{V_f}. \tag{3.3.1}$$

The above equation suggests that L_s is inversely proportional to V_f, in other words, L_s decreases with increasing V_f. V_f is much concerned with oxygen concentration, and increasing oxygen concentration accelerates the flame spread. This is because the flame temperature is increased with oxygen concentration, thereby leading to higher incident heat flux from the flame. Consequently, V_f increases with oxygen concentration, resulting in shorter L_s. It can also be seen that the preheat zone of CFRP [2×12cm] was larger

than that of CFRP [3×12cm] when comparing them at the same θ. For CFRP [2×12cm], there is no heated area other than the combustion area, whereas for CFRP [3×12cm], 5 mm in both sides is sandwiched by the sample holder. More heats are, therefore, transferred forward in CFRP [2×12cm] without heat losses sideways, resulting in longer L_s.

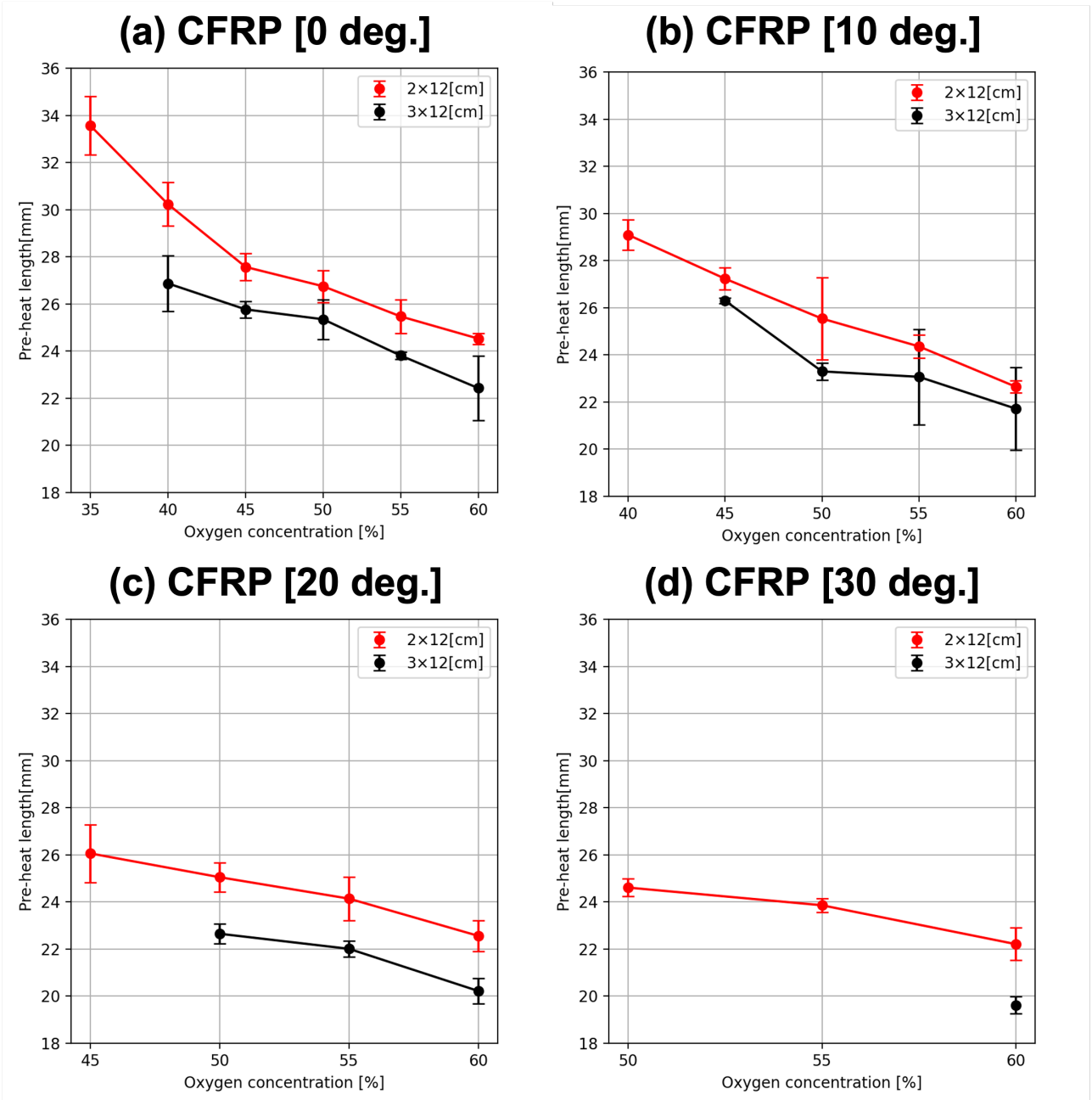

Fig. 3.3 Solid-phase preheat length of CFRP sheets at CF orientation angles of (a) 0 deg., (b) 10 deg., (c) 20 deg., and (d) 30 deg.

3.4. Flame length

Flame length (L_f) is one of the important characteristics for conductive heat transfer because residues under a flame, e.g., the half-burned CFs in this work, are heated to transfer heats forward. Therefore, the conductive heat flux increases as L_f becomes longer. L_f was then measured by applying the same in-house

Python image-processing code as that used for calculating L_s. As shown in Fig. 3.4, L_f became shorter and longer as θ and oxygen concentration are increased, respectively. L_f would be proportional to mass flux of fuel vapors. As mentioned in Section 3.2, the net conductive heat transfer rates, which contribute to the flame spread, decrease with increasing θ because of increased heat losses sideways. Lower heat transfer rates only produce lower mass flux of fuel vapors, and therefore L_f becomes shorter as θ is increased. On the other hand, increasing oxygen concentration elevates the flame temperature to facilitate the pyrolysis. Consequently, the mass flux of fuel vapors is increased with oxygen concentration, resulting longer L_f. In addition, L_f of CFRP [2×12cm] was longer than that of CFRP [3×12cm] at the same θ. The incident heat transfer rate from the flame would be higher in CFRP [2×12cm], and therefore more fuel vapors are produced to yield longer L_f.

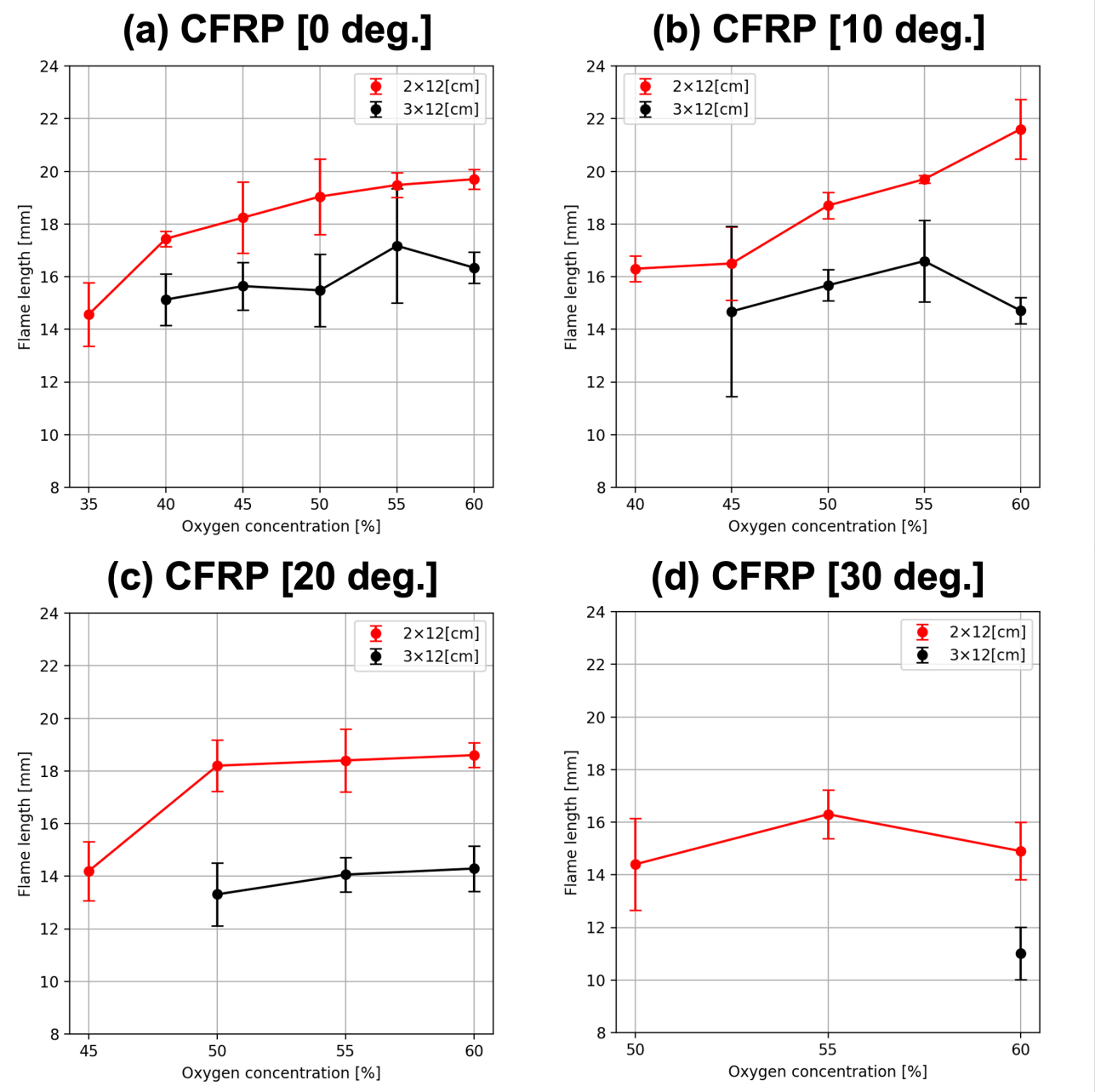

Fig. 3.4 Flame length of CFRP sheets at CF orientation angles of (a) 0 deg., (b) 10 deg., (c) 20 deg., and (d) 30 deg.

3.5. Flame spread rate

Flame spread rate (V_f) was measured by tracking the flame leading edge via an in-house Python image-processing code. V_f decreased as θ increased and increased as the oxygen concentration increased in Fig. 3.5. As A increases, the V_f is considered to decrease because the flame spread in the longitudinal direction of the sample is suppressed due to the decrease in L_s. V_f rate is also considered to increase as the oxygen concentration increases, because the higher oxygen concentration increases the flame temperature and the amount of heat transferred through the carbon fiber. In addition, $V_f$of CFRP [2×12cm] was higher than that of CFRP [2×12cm] at all the tested θ. This may be because some of the heat was used to increase the temperature in the non-burned zones of the CFRP [3 x 12 cm]. This is discussed in the next chapter as well using a model.

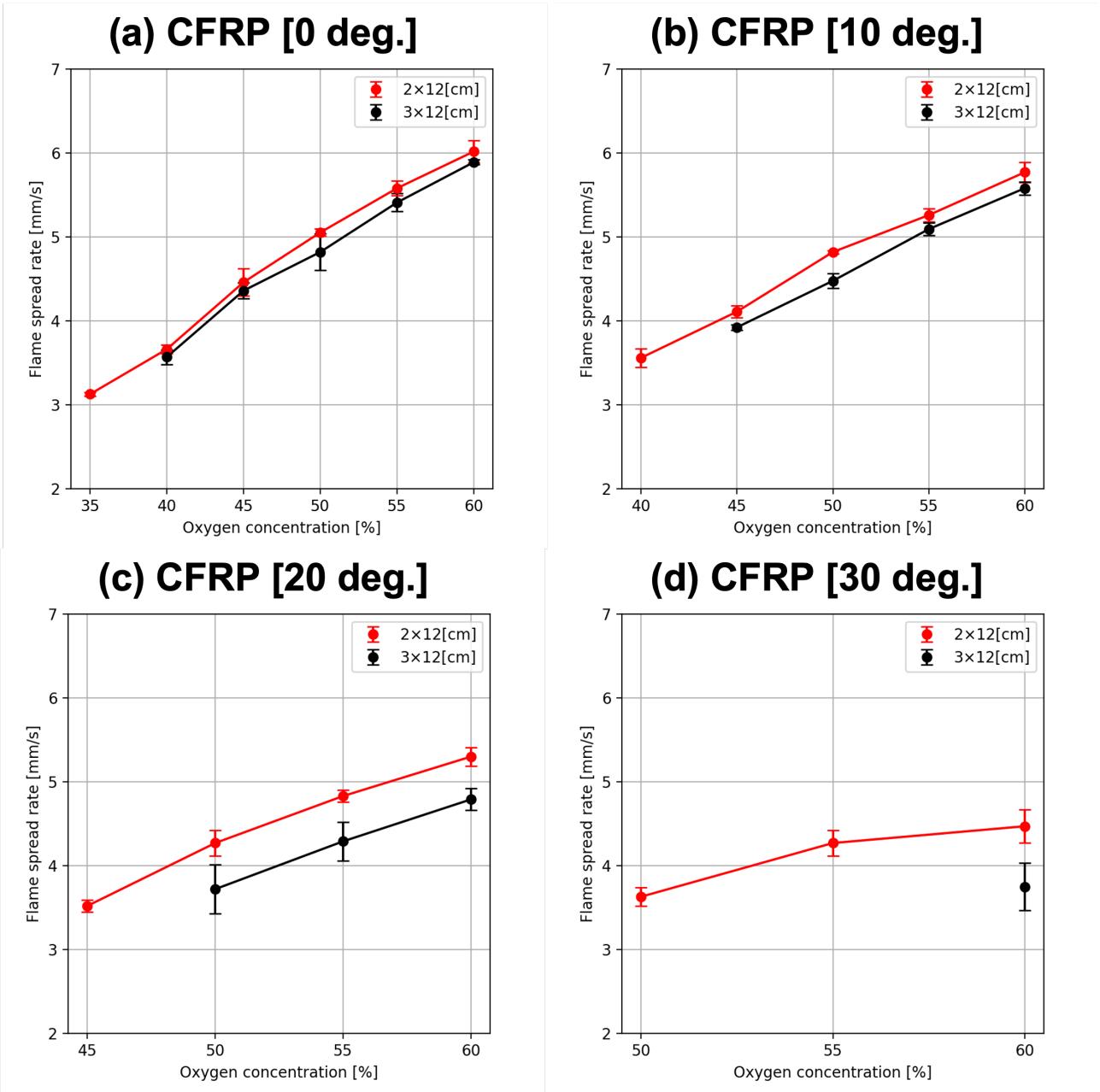

Fig. 3.5 Flame spread rate of CFRP sheets at CF orientation angles of (a) 0 deg., (b) 10 deg., (c) 20 deg., and (d) 30 deg.

4. Discussion

4.1. Conventional simplified flame spread model

The following simplified flame spread model was proposed by Kobayashi et al[5]. The possible heat transfer rates involve

Q_1, Q_2: incident heat transfer rates from flame (convection and radiation), and
Q_3, Q_4: heat transfer rates through the material.

Note that this model does not consider the forward gas-phase heat transfer because it is low enough to be negligible as compared to the solid-phase heat transfer (Q_2 and Q_4).

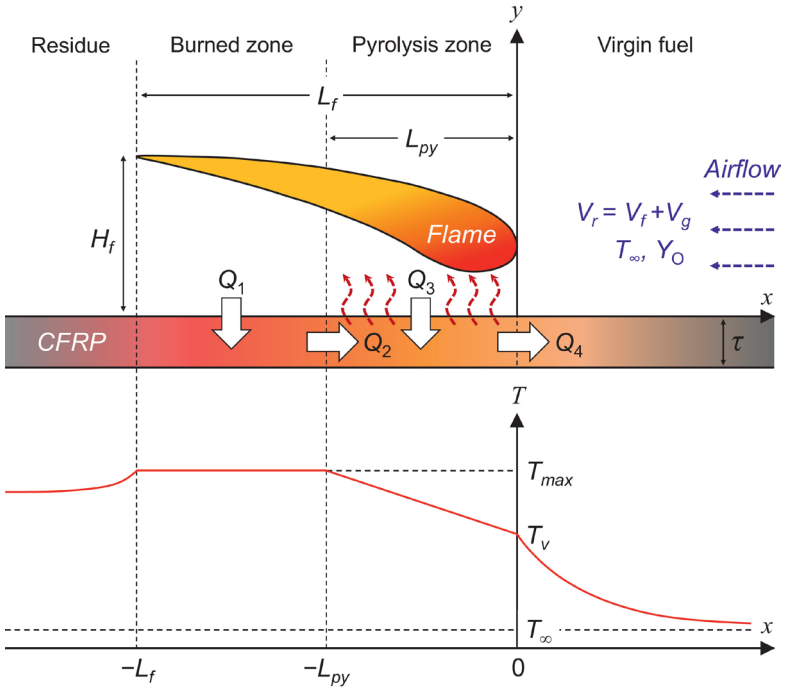

Fig. 4.1 Schematic of simplified flame spread model involving the solid-phase heat transfer with simulated surface temperature profile.

Nomenclature

V_f	: flame spread rate	τ	: material thickness
ρ_g	: gas-phase density	T_f	: flame temperature
ρ_s	: solid-phase density	T_{max}	: maximum temperature
c_g	: gas-phase specific heat	T_v	: pyrolysis temperature
c_s	: solid-phase specific heat	L_v	: latent heat of vaporization
λ_g	: gas-phase thermal conductivity	L_f	: flame length
λ_s	: solid-phase thermal conductivity	L_{py}	: pyrolysis zone length
α_g	: gas-phase thermal diffusivity	H_f	: flame height
α_s	: solid-phase thermal diffusivity	L_g	: thermal diffusion length

Formulating energy balance in each zone gives the following equations:

In burned zone:

$$Q_1 = Q_2 \tag{4.1.1}$$

In pyrolysis zone:

$$\rho_s c_s \tau V_f L_v = Q_2 + Q_3 - Q_4 \tag{4.1.2}$$

Eq. (4.1.1) does not involve conductive heat loss backward from the flame, i.e., downstream, because this model assumes that the high temperature of the burned material is still maintained behind the flame. The flame incident heat in the burned zone (Q_1) is therefore transferred to the pyrolysis zone through the material. Substituting Eq. (4.1.1) into Eq. (4.2.2) to eliminate the conductive heat transfers (Q_2) yields an analytical solution of flame spread rate as:

$$V_f = \frac{(Q_1 + Q_3) - (Q_4)}{\rho_s \tau L_v} \tag{4.1.3}$$

$$Q_4 = \rho_s c_s (T_v - T_\infty) \tau V_f \tag{4.1.4}$$

$$V_f = \frac{Q_1 + Q_3}{\rho_s \{c_s (T_v - T_\infty) + L_v\} \tau} \tag{4.1.5}$$

$$Q_1 = \lambda_g \frac{T_f - T_{max}}{H_f} \left(L_f - L_{py}\right) \tag{4.1.6}$$

$$Q_3 = \lambda_g \frac{T_f - T_v}{H_f} L_{py} \tag{4.1.7}$$

which suggests that the CFs just work as a heat conductor to transfer the heat flux forward, and that the flame spread over CFRP is driven by the flame heat flux transferred by the CFs. We then have only to consider the incident heat transfer rates from the flame. Here, referring to the simulated surface temperature profile in Fig. 4.1, the solid-phase heat transfer rate from the burned zone to the pyrolysis zone (Q_2) is represented as:

$$Q_2 = \lambda_s \frac{T_{max} - T_v}{L_{py}} \tau \tag{4.1.8}$$

From Eqs. (4.1.1), (4.1.6), and (4.1.8), the maximum temperature (T_{max}) is then:

$$T_{max} = \frac{\lambda_g \left(L_f - L_{py}\right) L_{py} T_f + \lambda_s \tau H_f T_v}{\lambda_g \left(L_f - L_{py}\right) L_{py} + \lambda_s \tau H_f} \tag{4.1.9}$$

Although the flame length (L_f) is measured as shown in Fig. 3.3, the flame height (H_f) and the length of the pyrolysis zone (L_{py}) are not experimentally obtained. However, closed-form expressions for flame geometry in opposed-flow flame spread were suggested by Bhattacharjee et al.[7], and Hf and L_{py} are given by the following equations:

$$H_f = \frac{1}{5} \frac{1}{Y_O} \frac{T_f - T_v}{T_v - T_\infty} L_g \tag{4.1.10}$$

$$L_{py} = \frac{1}{2} \frac{L_v}{c_s (T_v - T_\infty)} \frac{T_f - T_v}{T_v - T_\infty} L_g \tag{4.1.11}$$

However, this model does not consider the effect of the CF orientation and the non-burned zones in both sides held by the sample holder. Therefore, a new simplified flame spread model is proposed in Section 4.2.

4.2. Revised CFRP flame spread model

The thermal conductivity (λ_s) of CFRP used in the model in Fig. 4.1 is for $\theta = 0$ deg., and other θ is not mentioned. Here, we propose a thermal conductivity according to θ ($\lambda_{s,\theta}$). $\lambda_{s,\theta}$ is geometrically formulated as:

$$\lambda_{s,\theta} = \lambda_{s,0} \times \cos\left(\frac{\theta}{2}\right),$$

where $\lambda_{s,0}$ is 347 W/m/K at $\theta = 0$deg. The heat losses sideways Q_5 is written as:

$$Q_5 = \rho_s c_s (T_v - T_\infty)\tau V_f. \tag{4.2.1}$$

Here, the temperature in the unburned zones is assumed to reach the pyrolysis temperature. Assuming that the width of the combustion zone is a and the width of the noncombustion zone is b, and adapting Eq. (4.2.1) to the model in Fig. 4.1, we obtain

$$V_f = \frac{(aQ_1 + aQ_3) - (aQ_4 + bQ_5)}{a\rho_s \tau L_v} \tag{4.2.2}$$

$$V_f = \frac{a(Q_1 + Q_3)}{\rho_s\{(a+b)c_s(T_v - T_\infty) + aL_v\}\tau}. \tag{4.2.3}$$

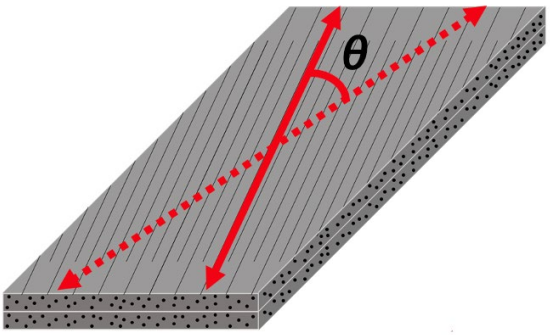

Fig. 4.2 Schematic of the CFRP sheet at a CF orientation angle of θ deg.

Table 4.1 Thermal conductivity of CFRP sheets in the direction of flame spread.

$\lambda_{s,0}$ (W/m/K)	$\lambda_{s,10}$ (W/m/K)	$\lambda_{s,20}$ (W/m/K)	$\lambda_{s,30}$ (W/m/K)	$\lambda_{s,30}$ (W/m/K)
347	345.7	341.7	335.2	326.1

4.3. Validation of the revised flame spread model via the measured flame spread rate

To validate the developed flame spread model, V_f of CFRP sheets is calculated via that model with the physicochemical properties listed in Table 4.2 and compared with the measured V_f. A comparison between the calculated and measured V_f is shown in Fig. 4.3, 4.4. If plots are on the dashed line, the calculated V_f corresponds to the measured V_f. Most plots are close to the dashed line, and therefore the calculated V_f agree with the measured V_f very well. We evaluate the model in more detail. As shown in Table 4.1, λ_s was varied, but the position of the plots remained almost unchanged even at 30 deg., where the difference was the largest. In Figure 4.4, the plot is closer to a wavy line as θ is increased. This is thought to be because the temperature

rise in the non-burning zone approaches the pyrolysis temperature (670 K) as θ increases.

Table 4.2 Physicochemical properties of CFRP and air for calculating flame spread rate.

	τ (mm)	ρ_g (kg/m³)	ρ_s (kg/m³)	c_g (J/kg/K)	c_s (J/kg/K)	λ_g (W/m/K)	λ_s (W/m/K)	T_v (K)	L_v (MJ/k)
CFRP	0.22	_	1780	_	860	_	326.1-347	670	1.417
Air	_	0.201-0.219	_	1735-1896	_	0.0848-0.0892	_	_	_

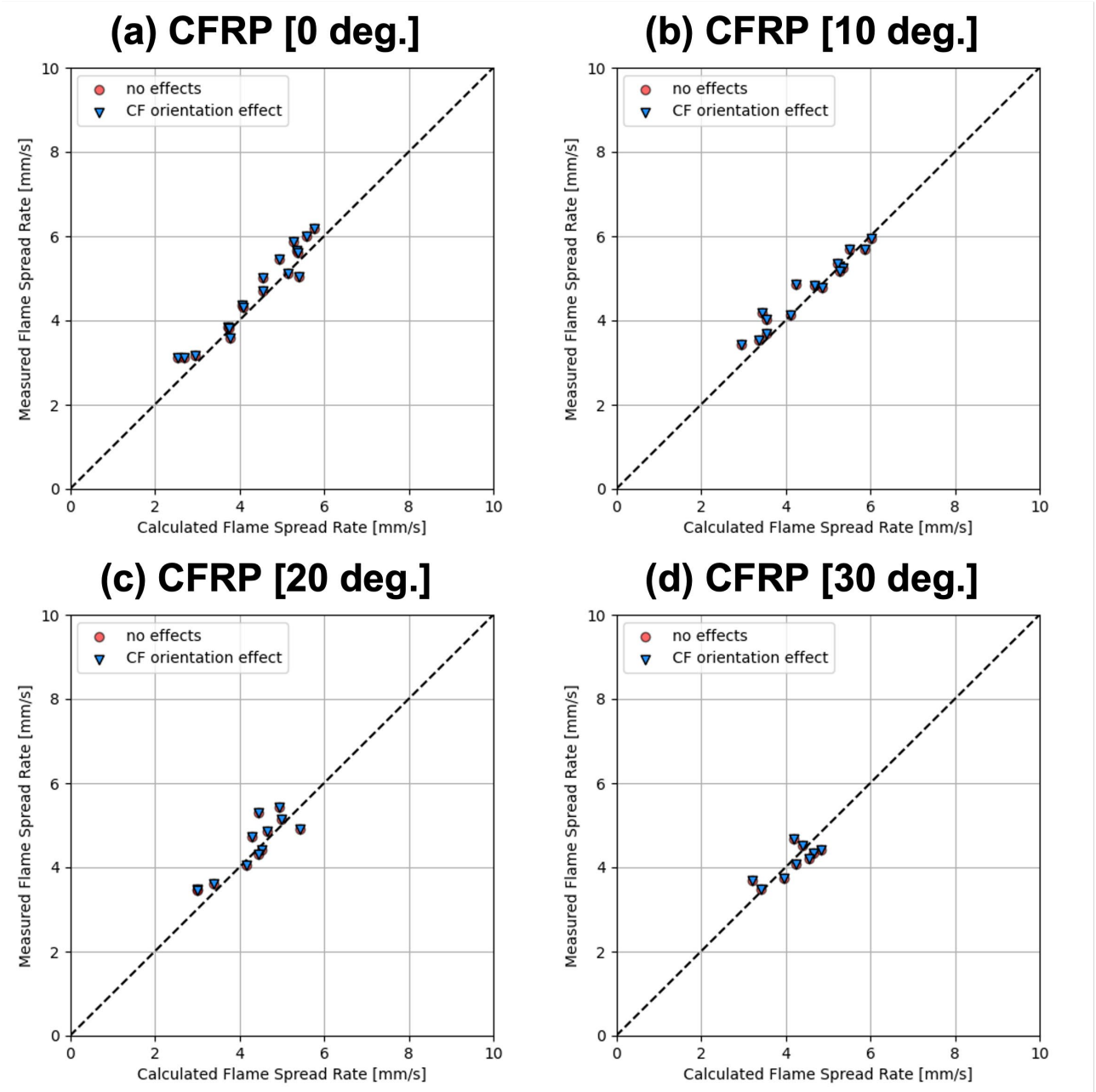

Fig. 4.3 Comparison of calculated and measured flame spread rates between the previous model and the newly developed model: (a) CFRP [0 deg.], (b) [10 deg.], (c) [20 deg.], and (d) [30 deg.] (CFRP [2 × 12 cm]).

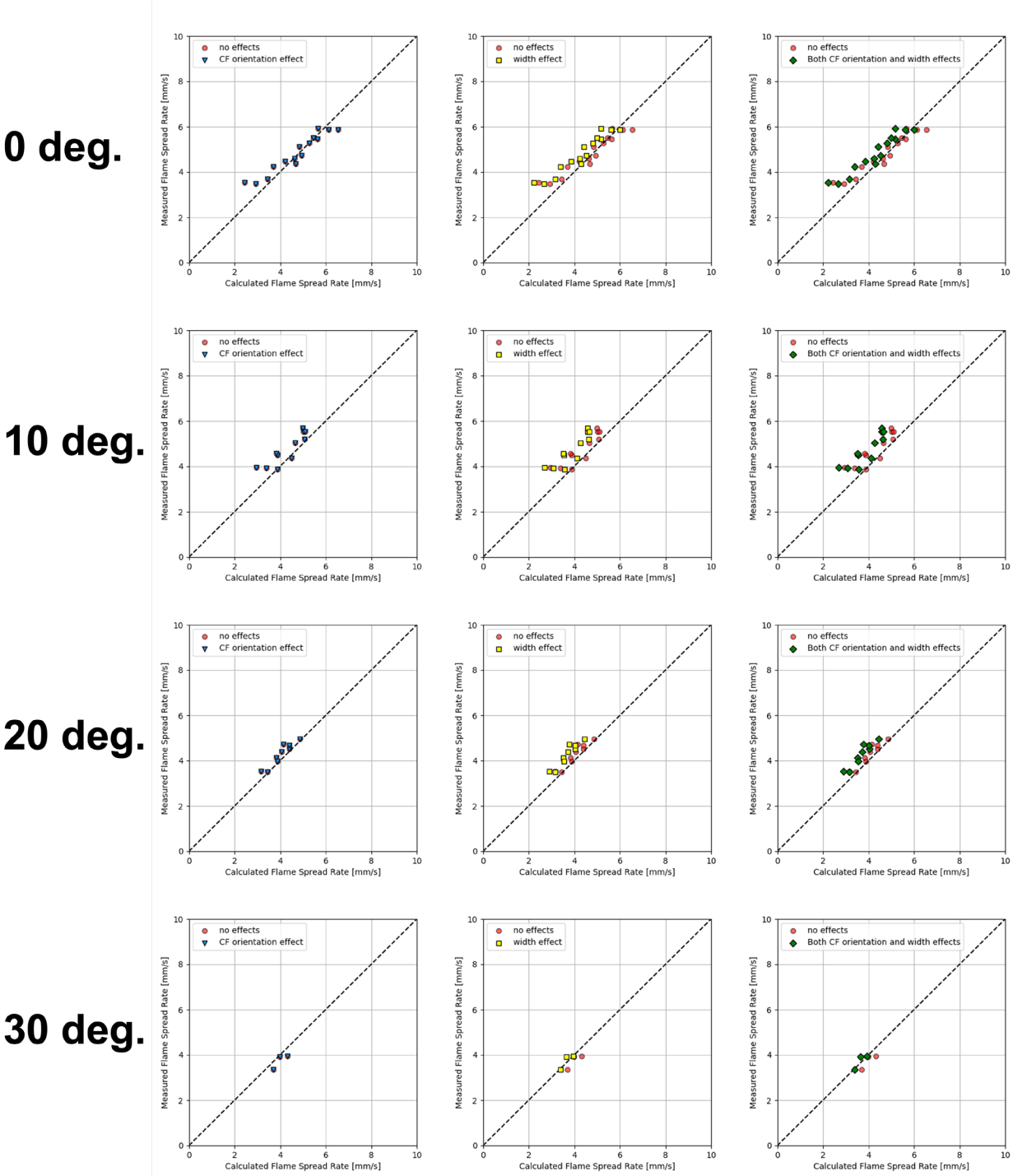

Fig. 4.4 Comparison of calculated and measured flame spread rate between the previous model and the newly developed model (CFRP [3 × 12 cm]).

5. Conclusions

This work studied the thermal influences of the non-burned regions on the opposed-flow flame spread over the CFRP sheets. Even if the area of the combustion zone is the same, the combustion characteristics change depending on the presence or absence of the no combustion zone. The flame spread rates calculated by the flame spread model of CFRP considering the unburned area well agreed with the measured flame spread rates.

References

1) A. C. Fernandez-Pello, S. R. Ray and I. Glassman: Flame spread in an opposed forced flow: the effect of ambient oxygen concentration. Symp. Combust., **18**, 1981, 579, DOI: https://doi.org/10.1016/S0082-0784(81)80063-X.
2) S. Takahashi, T. Ebisawa, S. Bhattacharjee and T. Ihara: Simplified model for predicting difference between flammability limits of a thin material in normal gravity and microgravity environments. Proc. Combust. Inst., **35**, 2015, 2535. DOI: https://doi.org/10.1016/j.proci.2014.07.017.
3) Y. Konno, N. Hashimoto and O. Fujita: Role of wire core in extinction of opposed flame spread over thin electric wires. Combust. Flame, **220**, 2020, 7. DOI: https://doi.org/10.1016/j.combustflame.2020.06.026.
4) Y. Kobayashi, K. Terashima, R. Oiwa and M. Tokoro: Opposed-flow flame spread over carbon fiber reinforced plastic under variable flow velocity and oxygen concentration: The effect of in-plane thermal isotropy and anisotropy. Proc. Combust. Inst., **38**, 2021, 4857. DOI: https://doi.org/10.1016/j.proci.2020.06.380.
5) Y. Kobayashi, R. Oiwa, M. Tokoro and S. Takahashi: Buoyant-flow downward flame spread over carbon fiber reinforced plastic in variable oxygen atmospheres. Combust. Flame, **232**, 2021, 111528. DOI: https://doi.org/10.1016/j.combustflame.2021.111528.
6) N. Matsukawa, K. Matsumoto, Y. Kobayashi and S. Takahashi: Downward flame spread over carbon fiber reinforced plastic with different carbon fiber orientations. 2021, OR2-3
7) S. Bhattacharjee, S. Takahashi, K. Wakai, C.P. Paolini: Correlating flame geometry in opposed-flow flame spread over thin fuels. Proc. Combust. Inst. **33**, 2011, 2465. DOI: https://doi.org/10.1016/j.proci.2010.06.053.

© 2022 by the authors. Submitted for possible open access publication under the terms and conditions of the Creative Commons Attribution (CC BY) license (http://creativecommons.org/li censes/by/4.0/).